



OPEN

Synthesis of (*E*)-2-(1*H*-tetrazole-5-yl)-3-phenylacrylenitrile derivatives catalyzed by new ZnO nanoparticles embedded in a thermally stable magnetic periodic mesoporous organosilica under green conditions

Sajedeh Safapoor, Mohammad G. Dekamin✉, Arezoo Akbari & M. Reza Naimi-Jamal

ZnO nanoparticles embedded in a magnetic isocyanurate-based periodic mesoporous organosilica ($\text{Fe}_3\text{O}_4@ \text{PMO-ICS-ZnO}$) were prepared through a modified environmentally-benign procedure for the first time and properly characterized by appropriate spectroscopic and analytical methods or techniques used for mesoporous materials. The new thermally stable $\text{Fe}_3\text{O}_4@ \text{PMO-ICS-ZnO}$ nanomaterial with proper active sites and surface area as well as uniform particle size was investigated for the synthesis of medicinally important tetrazole derivatives through cascade condensation and concerted 1,3-cycloaddition reactions as a representative of the Click Chemistry concept. The desired 5-substituted-1*H*-tetrazole derivatives were smoothly prepared in high to quantitative yields and good purity in EtOH under reflux conditions. Low catalyst loading, short reaction time and the use of green solvents such as EtOH and water instead of carcinogenic DMF as well as easy separation and recyclability of the catalyst for at least five consecutive runs without significant loss of its activity are notable advantages of this new protocol compared to other recent introduced procedures.

Since its first introduction by K. Barry Sharpless in 1999, “Click Chemistry (CC)” has been emerged as a very popular topic for the synthesis of heterocyclic compounds. In 2001, Sharpless defined CC reactions as a set of organic transformations with specific characteristics such as modular, wide in scope, affording high yields and produce only harmless byproducts that can be removed by non-chromatographic separation techniques¹⁻⁷. 1,3-dipolar cycloaddition reactions are one of the most popular CC reactions⁸. When such concerted reactions are performed through multicomponent reaction (MCR) strategy, they can be widely used for the synthesis of important heterocyclic compounds including triazole and tetrazole derivatives⁹⁻¹⁵.

The presence of four nitrogen atoms in the heteroaromatic five-membered ring of tetrazole gives rise to nitrogen-rich planar structural features¹⁶⁻²¹. Furthermore, the acidic nature of tetrazoles is due to the presence of free N-H in their structure and this property can lead to the formation of more complex aliphatic and aromatic heterocyclic compounds through nucleophilic substitution^{22,23}. Indeed, the heterocyclic tetrazole moiety can stabilize the negative charge of the corresponding anion by charge displacement and show same p*K*_a values of the corresponding carboxylic acids²⁴. As a result, tetrazoles can be used as a metabolic substitutes (bioisosteres) for the carboxylate functional group. Hence, these two groups of organic compounds are similar at p*K*_a = 4.9 and become deprotonated at physiological pH²⁵. Also, tetrazoles have higher nitrogen content than other heterocycles and require almost the same electronic space as carboxylates. Consequently, these features have improved their uses in a wide range of applications including pharmaceuticals and drug design, food industries, explosives, agrochemicals, materials science, coordination chemistry, etc.²⁶⁻³⁶. Especially, the tetrazole

Pharmaceutical and Heterocyclic Compounds Research Laboratory, Department of Chemistry, Iran University of Science and Technology, Tehran 16846-13114, Iran. ✉email: mdekamin@iust.ac.ir

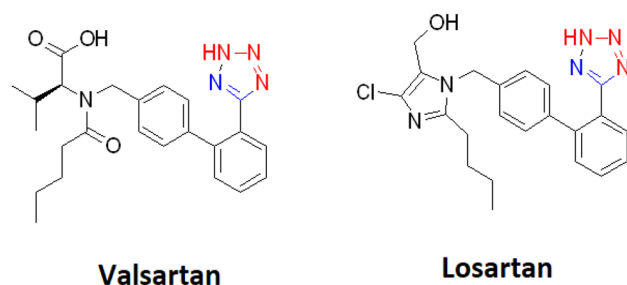


Figure 1. Valsartan and losartan as two active pharmaceutical ingredients with tetrazole moiety.

structures are similar to the pharmacological core of the Saran's family, which are in fact angiotensin II receptor blockers (ARB). Angiotensin II is a bioactive peptide that narrows the vessels through the contraction of the muscles around the heart³⁷. These drugs are used in to lower blood pressure and heart failure. Among the most important pharmaceuticals in this category of drugs are losartan and valsartan (Fig. 1). Indeed, these two active pharmaceutical ingredients are the first of a new class of drugs, which have been introduced for the clinical use in hypertension^{38,39}. Furthermore, many chemical studies on other tetrazole analogue compounds have described antibacterial and antifungal properties. Tetrazole derivatives also show anti-inflammatory, analgesic, anti-cancer, anticonvulsant and antidiabetic kidney disease activities³². Therefore, tetrazole chemistry has yet remained as a fascinating research area for different scientists.

Since the preparation of the first tetrazole compound in more than a hundred years ago, many scientists have invented or described different methods for preparation of tetrazole compounds³⁵. The most common of these methods is a 1,3-dipolar cycloaddition reaction between different simple nitrile derivatives and azide ion or hydrazoic acid under pressure. This approach has been more developed using different catalytic systems or altering of substrates during different decades^{35,40–42}. Some recent examples include the use of L-cysteine complex of palladium onto mesoporous channels of MCM-41⁴³, Fe₃O₄@L-lysine-Pd(0)⁴³, copper(I) salt²⁶, copper catalyst on biochar nanoparticles⁴⁴, guanidine complex of copper supported on boehmite nanoparticles⁴⁵, zinc(II) salts⁴⁶, Zn/Al hydrotalcite⁴⁷, NiFe₂O₄⁴⁸, TMSCl and Bu₂SnO or *N*-methyl-2-pyrrolidone⁴⁹, FeCl₃-SiO₂⁵⁰, Amberlyst-15²⁸, MCM-41-SO₃H⁵¹, 1-disulfo-[2,2-bipyridine]-1,1-dium chloride ionic liquid⁵² mainly at elevated temperatures, or dialkyl aluminum azides as the substrate and catalyst³⁶. Furthermore, Sharples and his colleague have reported improved intermolecular [3 + 2] ring closures between an azide and *p*-toluenesulfonyl cyanide or acyl cyanide under solvent-free conditions at elevated temperatures to afford good to excellent yields of the corresponding products using easy procedures^{53,54}. Moreover, the use of more complex nitrile derivatives such as benzylidenemalononitriles would be more desirable in terms of abundance of functional groups in the corresponding products⁵⁵. Indeed, this route for the synthesis of tetrazoles involves the multicomponent reactions (MCRs) strategy between aldehydes, sodium azide and nitriles. One of the advantages of this strategy is the use of available, easy and inexpensive basic compounds, namely aldehydes and sodium azide along with relatively expensive nitriles, which has made these reactions economically viable and easy to do on an industrial scale^{56–60}. Among different catalytic systems for benzylidenemalononitrile derivatives, which are generally prepared by condensation of aldehydes and molononitrile, Fe₃O₄@BNPs-CPTMS-Chitosan-Pd(0)⁶¹, Cu(II) immobilized on Fe₃O₄@HNTs-tetrazole nanocomposite⁶², secondary amine/Cu(II) bifunctional magnetic nanoparticles⁶³, Fe₃O₄ magnetic nanoparticles under microwave irradiation⁶⁴, NiO₂ nanoparticles⁶⁵, silica molybdic acid⁶⁶ and Cu₂(BDC)₂(DABCO) metal-organic framework⁶⁷ could be mentioned. In spite of their merits, there are some disadvantages to the most of previously reported protocols for the synthesis of tetrazoles. These include low boiling point of hydrazoic acid (37 °C), the use of expensive catalytic systems, high pressure conditions, toxic and carcinogenic solvents including DMF, or elevated temperature for the explosive azide ion component.

Periodic mesoporous organosilicas (PMOs) have been also emerged as one of the important issues of research in recent years. PMOs which were reported for the first time in 1999 are a new branch of mesoporous materials. They are organic-inorganic hybrid materials with high-ordered structures and uniform pore sizes^{68–82}. PMOs are essentially unique because of the advantage of combining a strong porous inorganic framework with the inherent properties of organic components having different functionalities^{71,83–86}. In this regard, precursors of bridged organosilica bearing hetero-aromatic isocyanurate moieties with high thermal stability and low toxicity would be very desirable^{82,85–88}. On the other hand, PMOs demonstrate other distinguishing characteristics such as large and hollow spaces, high surface area, regular cavity wall structure, low density and good membrane permeability, and material loading in large quantities. Therefore, PMOs have been effectively used in many applications such as drug and gene delivery, gas and molecule absorption, sensors, active agents for smart anticorrosive organic coatings, and catalysis^{85,86,89–107}.

To address the above challenges and in continuation of our studies to explore the catalytic activity of ZnO species^{108,109} as well as PMOs^{91,94–99}, we wish to report herein the new ZnO nanoparticles embedded in a magnetic isocyanurate-based periodic mesoporous organosilica (Fe₃O₄@PMO-ICS-ZnO) for the cascade reaction of different aromatic aldehydes and malononitrile to afford the corresponding Knoevenagel intermediate, and subsequent [3 + 2] cycloaddition with sodium azide (Fig. 2). Indeed, diverse tetrazole derivatives **5a–o** were prepared efficiently using low loading of Fe₃O₄@PMO-ICS-ZnO, as a magnetically recoverable catalytic system, in EtOH under reflux conditions in short reaction times.

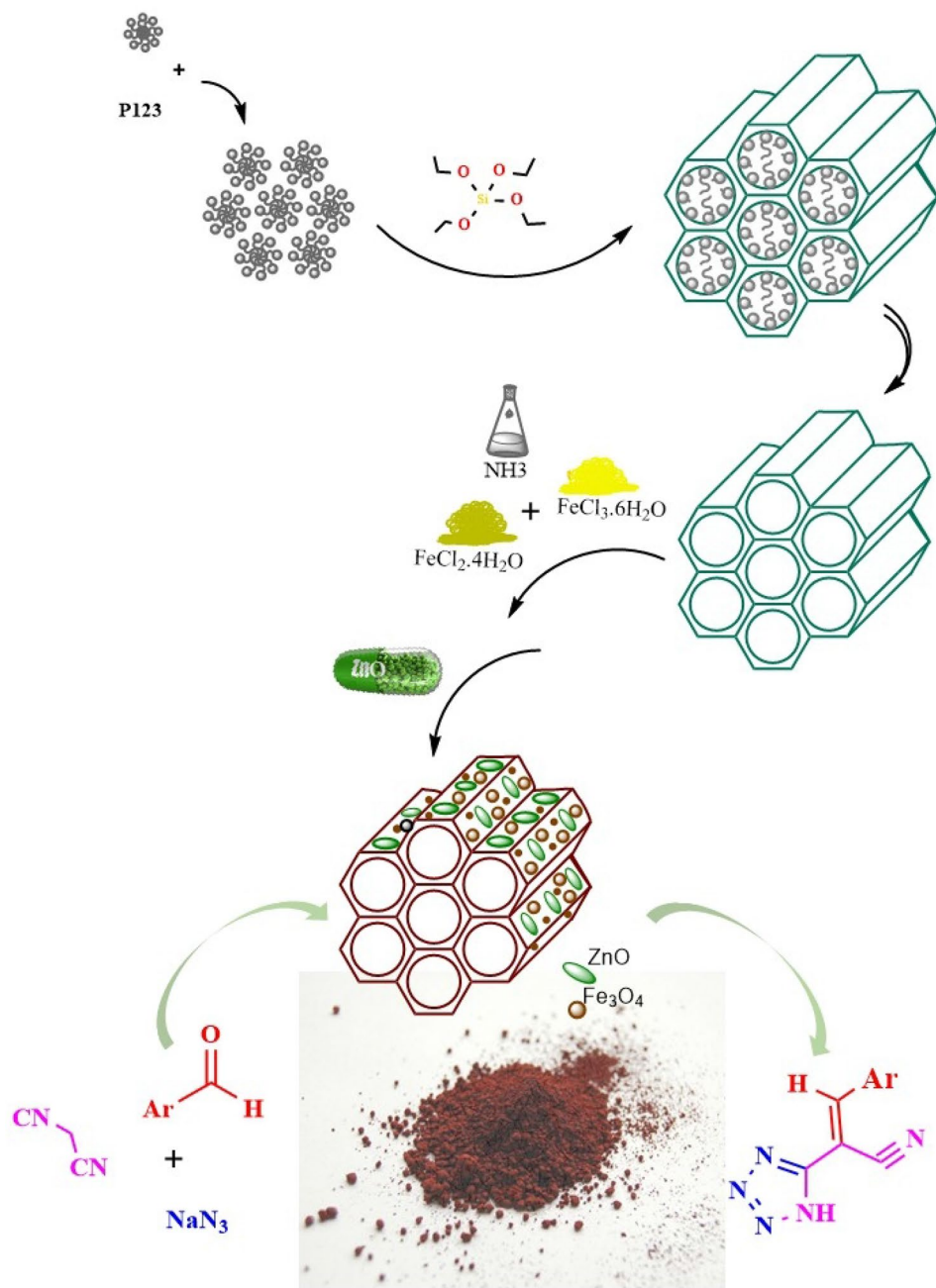


Figure 2. Schematic preparation of the Fe₃O₄@PMO-ICS-ZnO (1) catalyst and its application in the synthesis of tetrazoles derivatives 5a–o.

Results and discussion

After preparation of the Fe₃O₄@PMO-ICS-ZnO nanomaterial, its structural, morphological and textural properties were characterized by Fourier transform infra-red (FTIR) and X-ray powder diffraction (XRD) spectroscopy, field emission scanning electron (FESEM) microscopy, thermogravimetric analysis (TGA), N₂ adsorption–desorption isotherms and vibrating sample magnetometer (VSM).

The FT-IR spectra of both PMO-ICS and Fe₃O₄@PMO-ICS-ZnO have been presented in Fig. 3. It was observed that the free O–H stretching mode of the silanol groups on the PMO surface appear at 3415 cm⁻¹. Also, sharp absorption bands were observed at 1689 and 1471, which are related to the vibrations of carbonyl and C–N bonds in the isocyanurate ring within the framework of the prepared nanocatalyst, respectively. The signals appearing in 2939 and 2889 cm⁻¹ are related to the stretching vibrations of aliphatic moiety of PMO-ICS. Furthermore, the observed bands at 1108, 1056 and 943 cm⁻¹ correspond to the asymmetric and symmetric stretching vibrations of siloxane Si–O–Si bonds. On the other hand, the signals at 570 cm⁻¹ are related to the

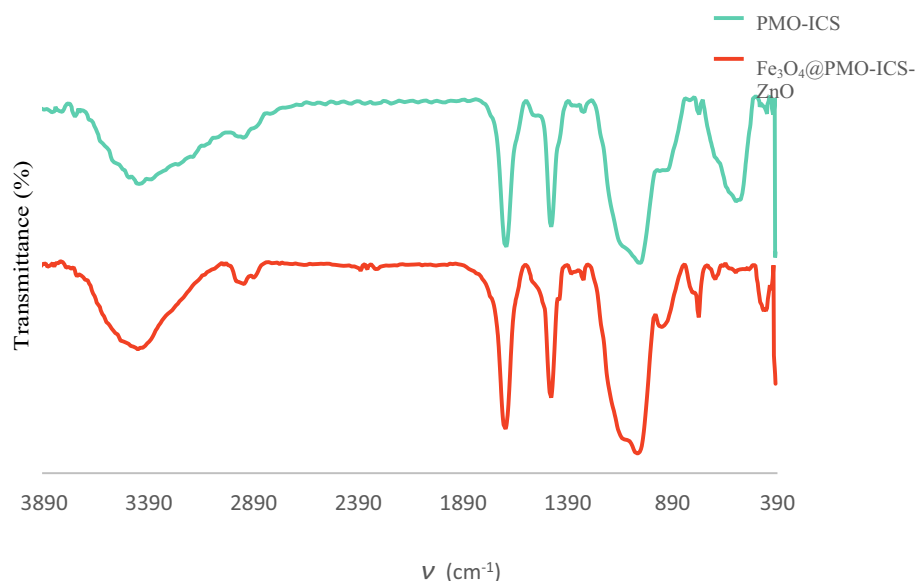


Figure 3. FTIR spectra of the PMO-ICS and magnetic Fe_3O_4 @PMO-ICS-ZnO nanoporous catalyst (**1**).

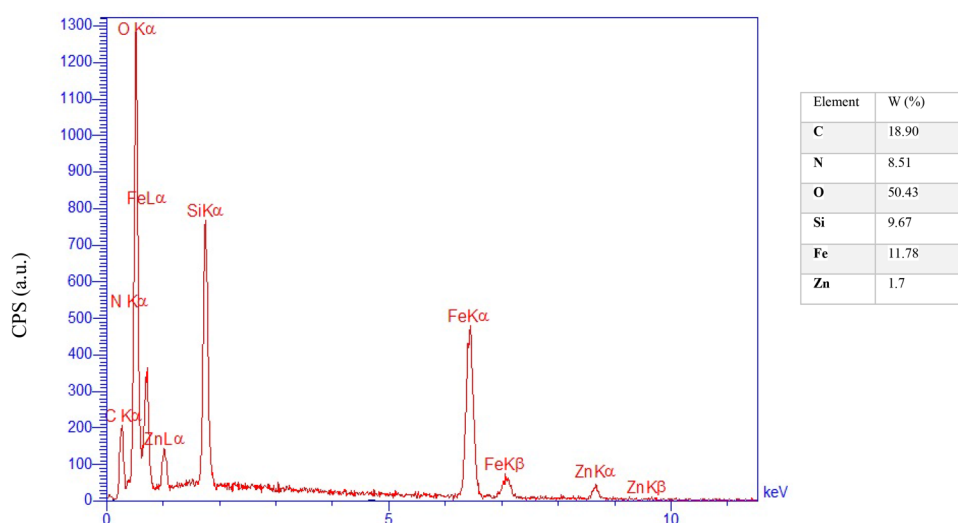


Figure 4. EDX spectrum of the magnetic Fe_3O_4 @PMO-ICS-ZnO mesoporous catalyst (**1**).

stretching vibration of the Fe–O–Fe bonds. The Zn–O stretching vibration modes are observed, as a relatively weak band at 493 cm^{-1} , which merge with the nearby signal of Fe–O bonds.

The energy dispersive X-ray (EDX) spectrum of the catalyst has been shown in Fig. 4. Indeed, the signals of iron, nitrogen, silicon, carbon, oxygen and zinc atoms were observed in the studied sample. It is well known that three peaks of iron are observed in the EDX spectrum for magnetic iron oxides. Furthermore, this analysis successfully confirms that ZnO nanoparticles are well embedded into the magnetic catalyst.

The structure of Fe_3O_4 @PMO-ICS-ZnO nanoparticles was also analyzed by XRD spectroscopy. The wide angle XRD pattern shown in Fig. 5 determined the crystallinity and arrangement of both PMO and Fe_3O_4 components in the structure of Fe_3O_4 @PMO-ICS-ZnO nanomaterial. Indeed, a broad diffraction peak of 2θ near to 3.9° and five sharp peaks at $2\theta = 29.5^\circ, 35.4^\circ, 43.2^\circ, 56.9^\circ,$ and 62.7° demonstrate corresponding reflections of amorphous silica as well as Fe_3O_4 and ZnO phases, respectively.

The morphology, distribution and size of the particles of Fe_3O_4 @PMO-ICS-ZnO nanoporous material (**1**) were analyzed using field emission scanning electron microscope (FESEM, Fig. 6). A uniform and well-defined distribution as well as almost nano-rod morphology were observed for the ZnO nanoparticles embedded in the magnetic periodic mesoporous organosilica. Furthermore, the average particle sizes of Fe_3O_4 @PMO-ICS-ZnO nanoporous material (**1**) was found to be in the range of nano scale and about 45–62 nm.

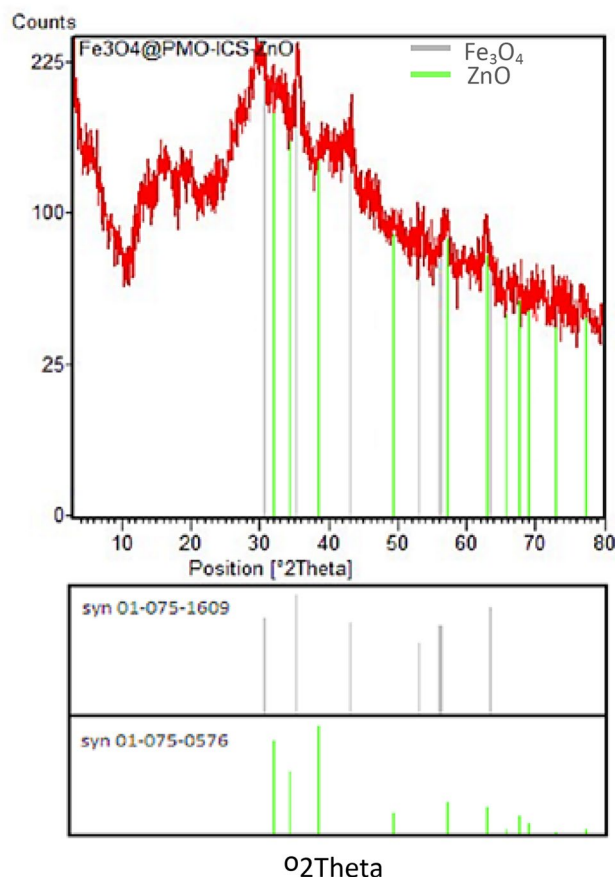


Figure 5. X-ray powder diffraction (XRD) pattern for the Fe_3O_4 @PMO-ICS-ZnO nanoporous catalyst (1).

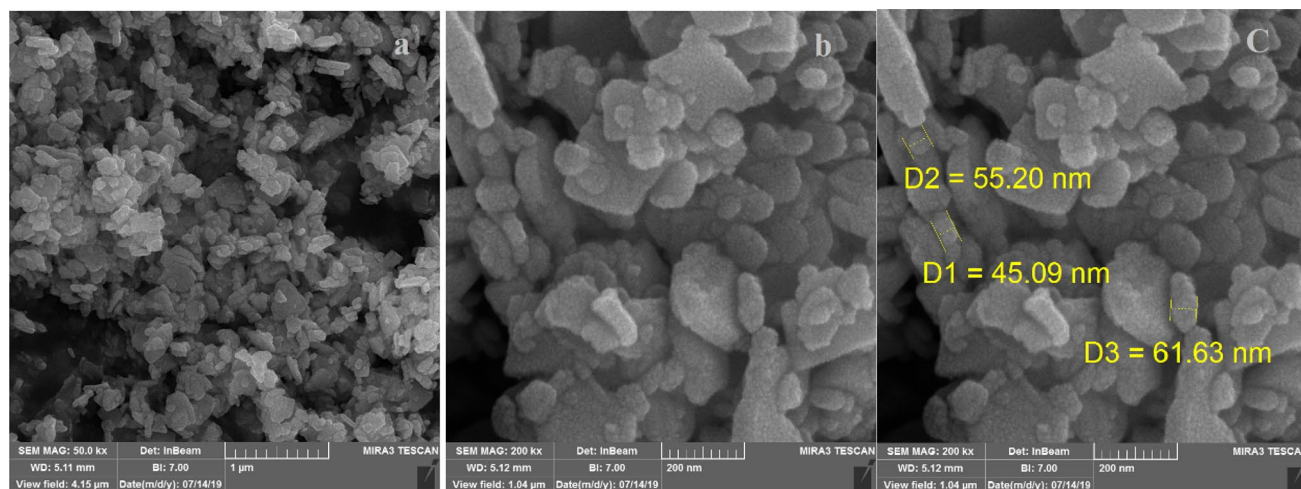


Figure 6. FESEM images of the magnetic nanoporous Fe_3O_4 @PMO-ICS-ZnO catalyst (1).

Furthermore, the specific surface area and pore size of nano-ordered Fe_3O_4 @PMO-ICS-ZnO material **1** were determined using N_2 adsorption–desorption isotherms through Brunauer–Emmett–Teller (BET) and Barrett–Joyner–Halenda (BJH) methods (Fig. 7). In fact, the observed data demonstrated that this material has a typical mesoporous structure and a type IV isotherm, which is due to the presence of cylindrical pores on the mesoporous scale. Specific surface area, average pore size and total pore volume are approximately $194.9 \text{ m}^2 \text{ g}^{-1}$, 7.3 nm , and $0.36 \text{ cm}^3 \text{ g}^{-1}$, respectively. Comparison of the obtained BET and BJH data of Fe_3O_4 @PMO-ICS-ZnO material **1** with the similar data for PMO-ICS⁸⁶ and Fe_3O_4 @PMO-ICS⁸⁷ shows decrease in the amount of surface area and total pore volume (Table 1). Therefore, it can be concluded that ZnO nanoparticles were firmly embedded and fixed in the magnetic periodic mesoporous organosilica channels.

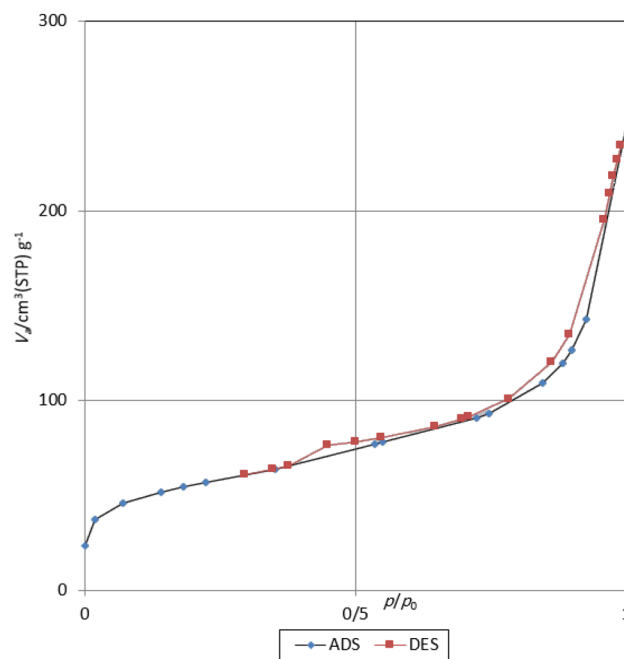


Figure 7. BET isotherm of the mesoporous $\text{Fe}_3\text{O}_4@PMO\text{-ICS-ZnO}$ nanocatalyst (**1**).

| Sample | BET surface area (m^2/g) | Total pore vol. (cm^3/g) (P/P_0 : 0.989) | Pore size (nm) |
|--|--|--|----------------|
| PMO-ICS | 570.03 | 5.0 | 4.160 |
| $\text{Fe}_3\text{O}_4@PMO\text{-ZnO}$ | 194.88 | 0.35 | 3.312 |

Table 1. Textural parameters of the PMO-ICS and $\text{Fe}_3\text{O}_4@PMO\text{-ICS-ZnO}$ (**1**) samples.

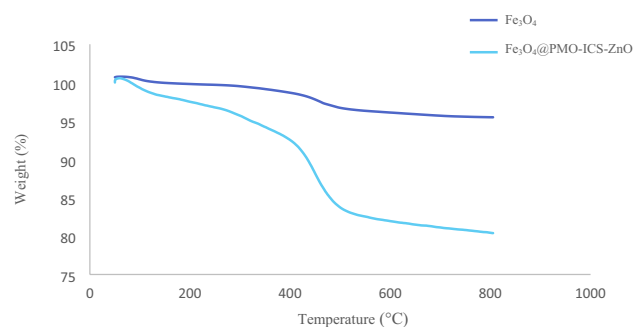


Figure 8. TGA curve of the $\text{Fe}_3\text{O}_4@PMO\text{-ICS-ZnO}$ catalyst (**1**).

Thermogravimetric analysis (TGA) was measured for the prepared catalyst **1** at temperatures between 40 and 804 °C. Figure 8 shows three distinct weight loss for the $\text{Fe}_3\text{O}_4@PMO\text{-ICS-ZnO}$ (**1**). The first step, with 3.56% weight loss between 40 and 270 °C, is corresponded to the removing of alcoholic or water solvents remaining from the extraction process. The second and main weight loss (14.20%) at 270 to 570 °C region is attributed to the elimination of 1,3,5-tris(1,3-propylen) isocyanurate bridges incorporated into the PMO framework as well as condensation of its silanol groups. Finally, the last weight loss (2.26%) was observed in the range of 570–804 °C, which is attributed to more condensation of inorganic moieties present in the structure of catalyst **1** including silica and ZnO. These data clearly shows good thermal stability of the $\text{Fe}_3\text{O}_4@PMO\text{-ICS-ZnO}$, which is very important in design and application of recyclable heterogeneous catalytic systems.

The magnetization of $\text{Fe}_3\text{O}_4@PMO\text{-ICS-ZnO}$ (**1**) sample was measured using vibrating sample magnetometer (VSM) experiment. As can be seen in the Fig. 9, the hysteresis phenomenon was not observed. Instead, the observed “S” like curve at room temperature is also a proof of the paramagnetism of the prepared $\text{Fe}_3\text{O}_4@PMO\text{-ICS-ZnO}$. The saturation magnetization value was strongly enhanced by the external magnetic field strength

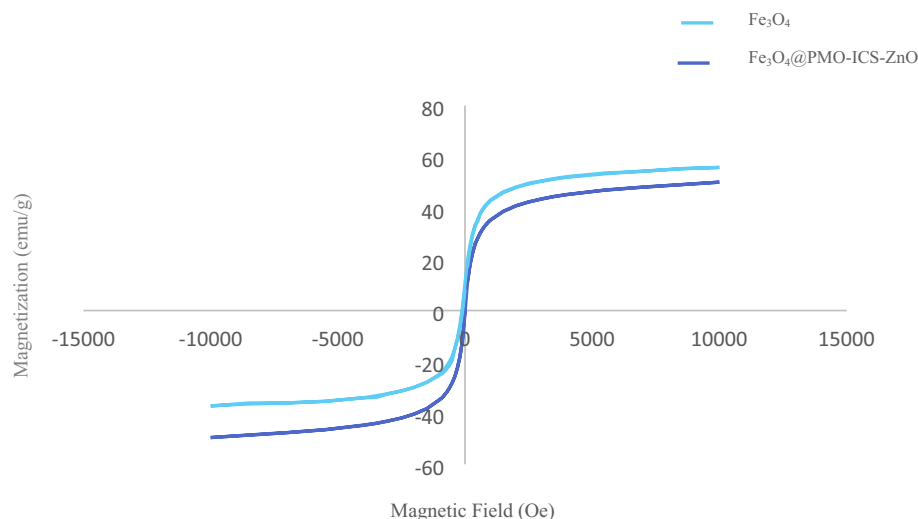


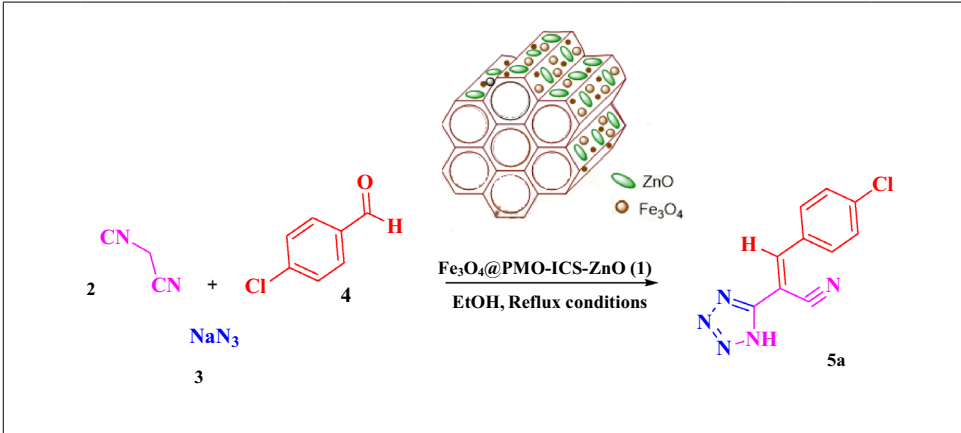
Figure 9. VSM magnetization curves for the Fe_3O_4 and $\text{Fe}_3\text{O}_4@PMO-ICS-ZnO$ (1).

at the low field region and found to be 49.56 emu/g for the $\text{Fe}_3\text{O}_4@PMO-ICS-ZnO$ at -10 to 10 KOe. Indeed, the magnetic property of the $\text{Fe}_3\text{O}_4@PMO-ICS-ZnO$ is sufficiently enough to be easily separated by an external magnet from the reaction mixture.

Optimization of conditions for the synthesis of tetrazole derivatives in the presence of magnetic $\text{Fe}_3\text{O}_4@PMO-ICS-ZnO$ nanocatalyst (1). After characterization of the magnetic $\text{Fe}_3\text{O}_4@PMO-ICS-ZnO$ nanocatalyst (1), its efficiency was investigated for the synthesis of 1*H*-tetrazole derivatives. Therefore, the effect of different catalyst loadings, solvent and temperature on the yield and required time of reaction were systematically investigated in this step to find optimal conditions for the synthesis of 1*H*-tetrazole derivatives. Hence, the reaction of malononitrile (2, 1 mmol) and sodium azide (3, 1.2 mmol) 4-chlorobenzaldehyde (4a, 1 mmol), was selected as the model reaction. The results have been summarized in Table 2. Initially, the model reaction was examined in the absence of any catalyst under various conditions such as in EtOH at ambient temperature or under reflux conditions. The dependence of obtained yield of the model reaction to the catalyst and temperature was evident because of very low yields of the desired product, (*E*)-3-(4-chlorophenyl)-2-(1*H*-tetrazol-5-yl)acrylonitrile, 5a under solvent-free conditions at room temperature or reflux conditions after prolonged reaction times (entries 1,2, Table 2). Interestingly, the obtained yield of desired product 5a was significantly improved in the presence of $\text{Fe}_3\text{O}_4@PMO-ICS-ZnO$ nanocatalyst (1) after very short reaction times (entries 3–5, Table 2). These findings demonstrate high catalytic activity of the magnetic nanocatalyst for the synthesis of the desired product 5a, which originates from very good dispersion of active catalytic sites and proper surface area of the $\text{Fe}_3\text{O}_4@PMO-ICS-ZnO$. In the next experiments, the effect of different solvents such as water, EtOH, water/EtOH mixture, toluene, DMF, EtOAc and CH_3CN as well as solvent-free conditions on the reaction rate was investigated (entries 6–12, Table 2). Indeed, both water and EtOH solvents afforded excellent yields of the desired product 5a after same reaction time (entries 5, 6, Table 2). However, separation of the magnetic catalyst 1 is much easier in EtOH than water due to higher solubility of the desired 1*H*-tetrazole products at elevated temperatures and remaining the heterogeneous catalyst 1. Therefore, 10 mg $\text{Fe}_3\text{O}_4@PMO-ICS-ZnO$ loading in EtOH under reflux conditions was selected as the optimized conditions for further experiments (entries 3, 13, 14, Table 2). On the other hand, both pure PMO-ICS and magnetic PMO-ICS afforded lower yields of the desired product 5a under similar conditions compared to the $\text{Fe}_3\text{O}_4@PMO-ICS-ZnO$ nanocatalyst (1) (entries 15, 16, Table 2). All of these data show effective role of ZnO nanoparticles embedded in the thermally stable magnetic periodic mesoporous organosilica.

In the next step, the optimized conditions were expanded to other aromatic aldehydes 4b–o to investigate the scope of reaction for the preparation of diverse 1*H*-tetrazole derivatives in the presence of magnetic $\text{Fe}_3\text{O}_4@PMO-ICS-ZnO$ nanocatalyst (1). Excellent yields were obtained from a variety of aromatic carbocyclic or heterocyclic aldehydes 4a–o under optimized conditions. As data in Table 3 show, high to excellent yields of the desired products 5a–o were obtained within short reaction times. In this regard, aromatic aldehydes with carbocyclic ring bearing electron withdrawing groups 4a–g and electron-deficient heterocycle 4h were examined (entries 1–8, Table 3). On the other hand, aromatic aldehydes with carbocyclic ring bearing electron donating groups 4j–n as well as electron-rich heterocycle 4o survived to involve in the optimized conditions to afford the corresponding 1*H*-tetrazole derivatives 5j–o (entries 10–15, Table 3).

Proposed mechanism for the preparation of 5-substituted-1*H*-tetrazole derivatives catalyzed by $\text{Fe}_3\text{O}_4@PMO-ICS-ZnO$ (1). A trajectory for the cascade one-pot preparation of (*E*)-2-(1*H*-tetrazole-5-yl)-3-aryl/heteroarylacrylenitrile derivatives 5a–o using Lewis acidic ZnO nanoparticles embedded in the



| Entry | Catalyst | Catalyst loading (mg) | Solvent | Temperature (°C) | Time | Yield ^a (%) |
|-------|--|-----------------------|-----------------------------|--------------------------|--------------|------------------------|
| 1 | – | – | Solvent-Free | rt | 24 h | 78 |
| 2 | – | – | EtOH | Reflux conditions | 20 h | 62 |
| 3 | Fe₃O₄@PMO-ICS-ZnO | 10 | EtOH | Reflux conditions | 3 min | 98 |
| 4 | Fe ₃ O ₄ @PMO-ICS-ZnO | 15 | EtOH | Reflux conditions | 5 min | 97 |
| 5 | Fe ₃ O ₄ @PMO-ICS-ZnO | 20 | EtOH | Reflux conditions | 5 min | 98 |
| 6 | Fe ₃ O ₄ @PMO-ICS-ZnO | 10 | H ₂ O | Reflux conditions | 5 min | 95 |
| 7 | Fe ₃ O ₄ @PMO-ICS-ZnO | 10 | H ₂ O/EtOH (1:1) | Reflux conditions | 40 min | 80 |
| 8 | Fe ₃ O ₄ @PMO-ICS-ZnO | 10 | Toluene | Reflux conditions | 45 min | 90 |
| 9 | Fe ₃ O ₄ @PMO-ICS-ZnO | 10 | DMF | Reflux conditions | 60 min | Trace |
| 10 | Fe ₃ O ₄ @PMO-ICS-ZnO | 10 | EtOAc | Reflux conditions | 30 min | 72 |
| 11 | Fe ₃ O ₄ @PMO-ICS-ZnO | 10 | CH ₃ CN | Reflux conditions | 10 min | 70 |
| 12 | Fe ₃ O ₄ @PMO-ICS-ZnO | 10 | Solvent-Free | 100 | 20 min | 97 |
| 13 | Fe ₃ O ₄ @PMO-ICS-ZnO | 10 | EtOH | 60 | 7 min | 86 |
| 14 | Fe ₃ O ₄ @PMO-ICS-ZnO | 10 | EtOH | rt | 10 min | 97 |
| 15 | PMO-ICS | 10 | EtOH | Reflux conditions | 45 min | 70 |
| 16 | Fe ₃ O ₄ @PMO-ICS | 10 | EtOH | Reflux conditions | 40 min | 78 |

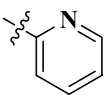
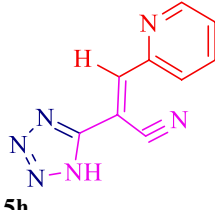
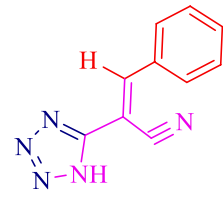
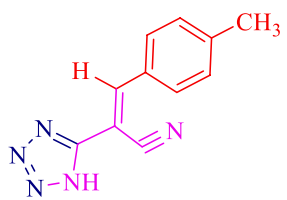
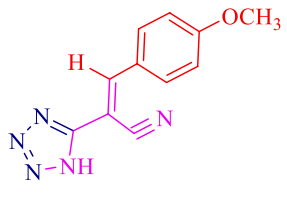
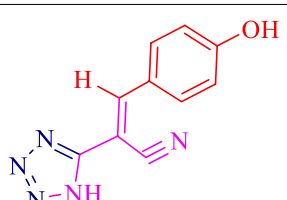
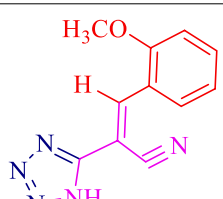
Table 2. Optimization of conditions in the reaction of malononitrile (2), NaN₃ (3) and 4-chlorobenzaldehyde (4a) under different conditions. Reaction conditions: malononitrile (2, 1 mmol), NaN₃ (3, 1.2 mmol) and 4-chlorobenzaldehyde (4a, 1 mmol) were added into the solvent (2.0 mL) in the presence of Fe₃O₄@PMO-ICS-ZnO (1) unless otherwise stated. ^aIsolated yields. Significant values are in bold.

magnetic isocyanurate-based periodic mesoporous organosilica (Fe₃O₄@PMO-ICS-ZnO, 1) is shown in Fig. 10. In the first reaction step, the aromatic aldehydes (4) are activated by the Fe₃O₄@PMO-ICS-ZnO step by step to condensate with the malononitrile C–H acid (2) and finally affording the Knoevenagel aryl/heteroarylidene malononitrile intermediate (III). This intermediate is subsequently involved in the concerted [3 + 2] cycloaddition with sodium azide (3) to produce 5-membered tetrazole ring.

Investigating of the reusability of magnetic Fe₃O₄@PMO-ICS-ZnO (1) for the synthesis of 5-substituted-1H-tetrazole derivatives 5. As a part of our study, the reusability of magnetic Fe₃O₄@PMO-ICS-ZnO (1) for the synthesis of (*E*)-3-(4-chlorophenyl)-2-(1H-tetrazol-5-yl)acrylonitrile 5a was investigated in the next step. The catalyst 1 was easily separated after completion of the model reaction under optimized conditions by an external magnet. The recycled Fe₃O₄@PMO-ICS-ZnO was separately dispersed in EtOH and EtOAc for 15 min, respectively. The recycled catalyst was kept in an oven at 60 °C for 1 h and then reused for the next runs. The results of the catalyst recycling for five consecutive runs are given in Fig. 11. As data in Fig. 10 demonstrate, only a slight decrease in reaction yield was observed after fourth run. These findings indicate the structural stability of magnetic the Fe₃O₄@PMO-ICS-ZnO (1) during synthesis of 5-substituted-1H-tetrazole derivatives 5.

Comparison of the catalytic activity of nano-ordered Fe₃O₄@PMO-ICS-ZnO (1) in the synthesis of tetrazole derivatives with other catalytic systems. Table 4 compares the previously reported methods for the synthesis of tetrazole 5a with the present protocol. It is apparent that high to excellent yields, avoiding the use of toxic or carcinogenic solvents such as DMF, short reaction time and easy separation of the catalyst from the reaction mixture are the advantages of the present protocol compared to the most of previously reported methods.

| Entry | Aldehyde 4 (Ar) | Product 5 | Time (min) | Yield ^a (%) | MP °C (Obs.) | MP °C (Lit.) |
|-----------|---|---------------|------------|------------------------|--------------|------------------------|
| 1 | 4-ClC ₆ H ₄ 4a | 5b | 5 | 98 | 157–159 | 158–160 ¹¹⁰ |
| 2 | 4-FC ₆ H ₄ 4b | 5b | 5 | 78 | 175–177 | 176–179 ¹¹¹ |
| 3 | 3-BrC ₆ H ₄ 4c | 5c | 5 | 80 | 162–163 | 165–167 ¹¹² |
| 4 | 2-ClC ₆ H ₄ 4d | 5d | 15 | 97 | 171–173 | 175–177 ⁶⁴ |
| 5 | 2,4-Cl ₂ C ₆ H ₃ 4e | 5e | 30 | 95 | 150–152 | 142–143 ¹¹³ |
| 6 | 4-NO ₂ C ₆ H ₄ 4f | 5f | 25 | 95 | 167–169 | 166–168 ¹¹² |
| 7 | 3-NO ₂ C ₆ H ₄ 4g | 5g | 30 | 92 | 161–163 | 159–163 ⁶⁶ |
| Continued | | | | | | |

| Entry | Aldehyde 4 (Ar) | Product 5 | Time (min) | Yield ^a (%) | MP °C (Obs.) | MP °C (Lit.) |
|-----------|--|--|------------|------------------------|--------------|------------------------|
| 8 |  4h |  5h | 8 | 88 | 187–188 | 185–186 ¹¹³ |
| 9 | C_6H_5 4i |  5i 5i | 5 | 97 | 165–167 | 168–170 ¹¹² |
| 10 | $4-CH_3C_6H_4$ 4j |  5j | 5 | 97 | 186–188 | 189–191 ¹¹⁴ |
| 11 | $4-MeOC_6H_4$ 4k |  5k | 20 | 90 | 150–152 | 153–155 ⁶⁶ |
| 12 | $4-HOC_6H_4$ 4l |  5l | 5 | 88 | 161–164 | 159–161 ¹¹² |
| 13 | $2-MeOC_6H_4$ 4m |  5m | 7 | 90 | 157–159 | 150–152 ¹¹⁵ |
| Continued | | | | | | |

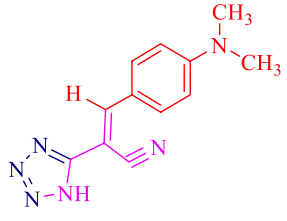

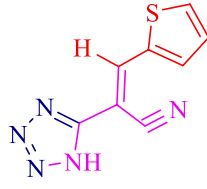
| Entry | Aldehyde 4 (Ar) | Product 5 | Time (min) | Yield ^a (%) | MP °C (Obs.) | MP °C (Lit.) |
|-------|--|--|------------|------------------------|--------------|------------------------|
| 14 | 4-Me ₂ NC ₆ H ₄ 4n |  5n | 25 | 88 | 167–168 | 171–172 ¹¹³ |
| 15 |  4o |  5o | 15 | 80 | 88–90 | 85–86 ¹¹³ |

Table 3. Synthesis of 5-substituted-1*H*-tetrazole derivatives **5a–o** catalyzed by the Fe₃O₄@PMO-ICS-ZnO nanocatalyst (**1**) via the three components reaction strategy. Reaction conditions: malononitrile (**2**, 1 mmol), aldehyde (**4**, 1 mmol), and NaN₃ (**3**, 1.2 mmol) were added into the EtOH (2.0 mL) in the presence of 10 mg of Fe₃O₄@PMO-ZnO (**1**). ^aIsolated yields.

Experimental

Reagents and instruments. All chemical substances and reagents with high purity were purchased from Merck or Aldrich and used as received, except for liquid aldehydes which were distilled before their using. The progress of reactions and the purity of the obtained products were monitored by thin layer chromatography (TLC) using Merck aluminum plates coated with 0.2 mm silica gel F254. Melting points were measured using an Electrothermal 9100 device and are uncorrected. Characterization of the magnetic catalyst **1** as well as identification of products was performed using KBr discs on a Shimadzu FTIR-8400S spectrometer. A Bruker DRX-500 Avance spectrometer was used for recording of ¹H NMR (500 MHz) and ¹³C NMR (125 MHz) spectra of products in DMSO-*d*₆ at ambient temperature. The BET specific surface area analysis was performed using ASAP 2020™ instrument. Thermal gravimetric analysis data was obtained by a Bahr company STA 504 equipment. X-Ray diffraction pattern was prepared using a STOE apparatus with CuKα radiation source. Field emission scanning electron microscopy images were recorded by a Zeiss (EM10C) device. VSM analysis was performed using a Lakeshore 7410 series instrument (Supplementary file).

Typical procedure for the preparation of PMO-ICS. The periodic mesoporous organosilica denoted PMO-ICS was prepared according to the method introduced by Jaroniec¹²². This PMO-ICS was synthesized by self-assembly of tris[3-(trimethoxysilyl)propyl] isocyanurate (ICS, Aldrich), tetraethyl orthosilicate (TEOS, Aldrich) in the presence of poly(ethylene oxide)-poly(propylene oxide)-poly(ethylene oxide) triblock copolymer (Pluronic 123, Aldrich, average Mw ≈ 5800 Dalton) under acidic conditions. In a typical experiment, P123 (2.0 g) was added into a 250 mL beaker and a mixture of deionized water (15 mL) and hydrochloric acid solution (2.0 M, 60 mL) was slowly added and stirred until P123 is completely dissolved. Then, ICS (0.01 mol, 3.08 g) and TEOS (0.03 mol, 3.12 g) were simultaneously added dropwise into the obtained solution. After that, the obtained white gel and precipitates was stirred at room temperature for 24 h in a round bottom flask. Then, the mixture was aged at 100 °C for 48 h without stirring. The solid was filtered off and washed thoroughly with hot EtOH/HCl (60 mL of 96% EtOH and 2 mL of 12.0 M HCl) using a soxhlet apparatus for 72 h to remove the surfactant molecules. The obtained white powder was finally dried in air at 100 °C overnight.

General procedure for the preparation of magnetic Fe₃O₄@PMO-ICS. PMO-ICS (2.0 g) was dispersed in toluene (20 mL) at room temperature. After 15 min stirring, FeCl₂·4H₂O (2.0 g) and FeCl₃·6H₂O (4.0 g) were added to the above mixture under nitrogen atmosphere. The reaction mixture was heated in an oil bath at 80 °C during stirring. Then, ammonia solution (25% w/w, 20 mL) was added dropwise into the mixture over a period of 30 min until pH 11.0 is reached and allowed to stir for one hour at the same temperature. The obtained black precipitate was finally collected by an external magnet, washed with deionized water and EtOH and then dried at 100 °C for 2 h.

Preparation of ZnO nanoparticles embedded in the mesoporous Fe₃O₄@PMO-ICS (Fe₃O₄@PMO-ICS-ZnO, **1).** At this stage, Zn(OAc)₂ in the presence of PEG-600 surfactant was used to embed

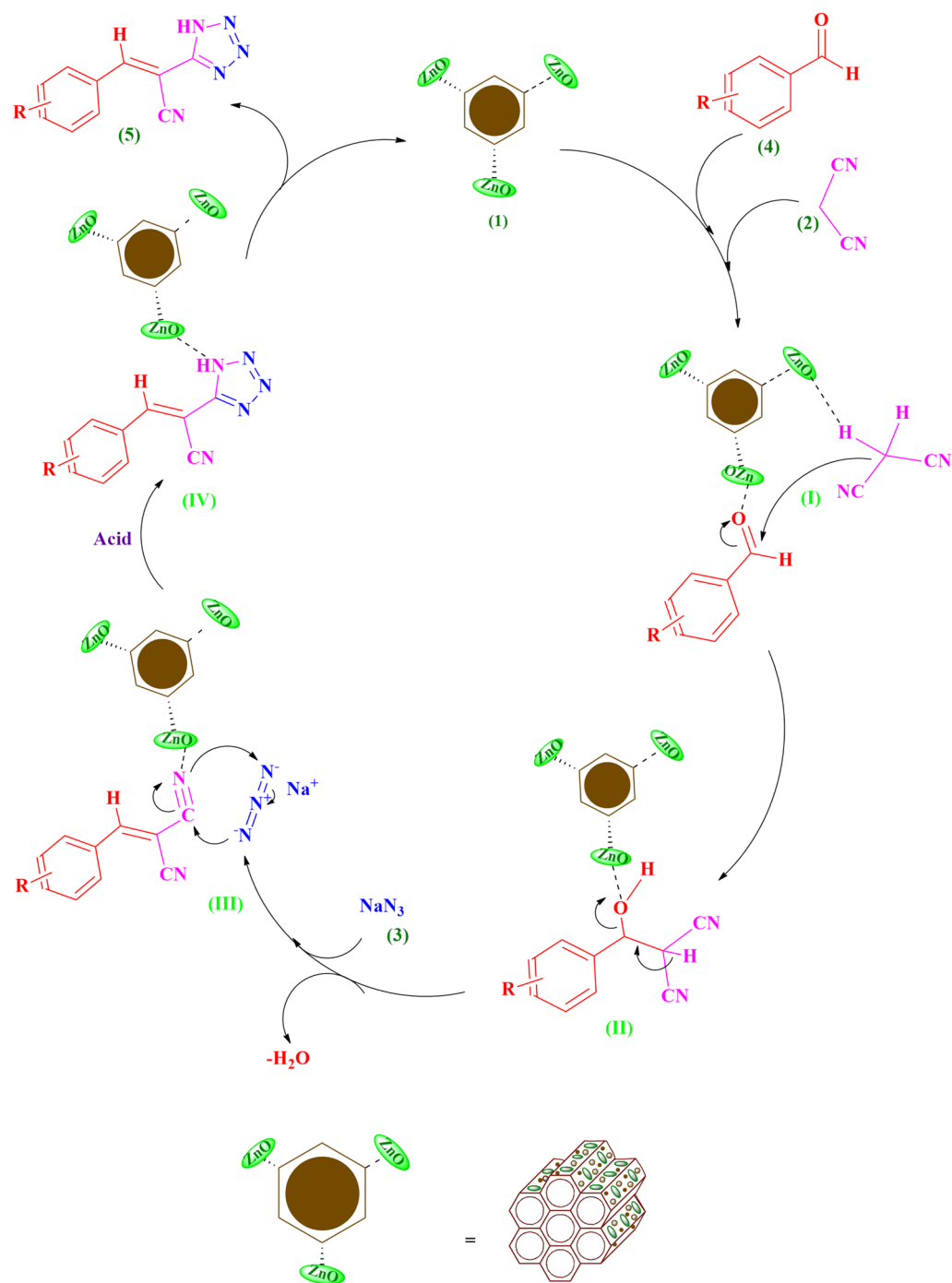


Figure 10. A reasonable mechanism for the one-pot preparation of (*E*)-2-(1*H*-tetrazole-5-yl)-3-aryl/heteroarylacrylenitrile derivatives **5** using the magnetic nano-ordered $\text{Fe}_3\text{O}_4@PMO\text{-ICS-ZnO}$ catalyst (**1**).

ZnO nanoparticles into the channels of $\text{Fe}_3\text{O}_4@PMO\text{-ICS}$. $\text{Zn}(\text{OAc})_2$ (0.1 g) and PEG (0.1 g) were added to a mixture of $\text{Fe}_3\text{O}_4@PMO\text{-ICS}$ (3.0 g) dispersed in twice-distilled water (50 mL). Then, NH_3 solution (25% w/w) was added dropwise to the obtained mixture and adjusting pH to 10.0 and then heated for 8 h at 80 °C. Finally, the mixture was cooled to ambient temperature and the obtained crimson $\text{Fe}_3\text{O}_4@PMO\text{-ICS-ZnO}$ powder was magnetically separated. The powder was washed with deionized water twice and then dried at 100 °C for 2 h.

General procedure for the synthesis of 5-substituted-1*H*-tetrazoles derivatives **5a-o catalyzed by $\text{Fe}_3\text{O}_4@PMO\text{-ICS-ZnO}$ (**1**).** In a single-neck round-bottom 10 mL flask equipped with a condenser, a mixture of malononitrile (**2**, 1 mmol), sodium azide (**3**, 1.2 mmol) and aldehyde (**4**, 1 mmol) was heated in the presence of $\text{Fe}_3\text{O}_4@PMO\text{-ICS-ZnO}$ catalyst **1** (10 mg) in EtOH under reflux conditions for the time indicated in Table 3. The reaction progress was monitored by TLC (Eluent: EtOAc/*n*-hexane, 1:3). After completion of

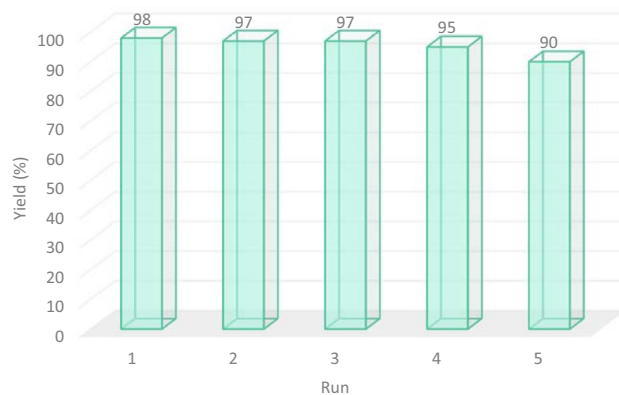


Figure 11. Reusability data for the magnetic $\text{Fe}_3\text{O}_4@PMO\text{-ICS-ZnO}$ mesoporous catalyst (1) in the synthesis of **5a**.

| Entry | Catalyst | Catalyst loading (mg) | Conditions | Time (h) | Yield 4a (%) | Ref. |
|-------|---|-----------------------|-------------------------------------|----------|---------------------|------------------|
| 1 | NiO nanoparticles | 4.5 | DMF/70 °C | 6 | 87 | ⁶⁵ |
| 2 | Silica molybdic acid | 200 | H ₂ O/MW/50 °C | 20 min | 91 | ⁶⁶ |
| 3 | Zn (Metallic) | 130.7 | H ₂ O/50 °C | 3 | 68 | ¹¹⁰ |
| 4 | Fe(OAc) ₂ | 17.4 | DMF/H ₂ O (9:1) 80 °C | 24 | 89 | ¹¹⁶ |
| 5 | (CuOTf) ₂ ·C ₆ H ₆ | 36.2 | Toluene/rt | 7 | 81 | ¹¹⁷ |
| 6 | Montmorillonite K 10 | 10.0 | H ₂ O | 17 | 29 | ¹¹⁸ |
| | | | DMF | | 38 | |
| 7 | Cu(OAc) ₂ | 45.4 | DMF/120 °C | 12 | 96 | ¹¹⁹ |
| 8 | Catalyst-Free | — | Solvent-Free | 24 h | 78 | — |
| 9 | OPNSA | 45.4 | Solvent-Free | 8 | 90 | ¹²⁰ |
| 10 | H ₃ PW ₁₂ O ₄₀ | 20.2 | Solvent-Free/120 °C | 6 | 93 | ¹²¹ |
| 11 | NH-Cu(II)@MNP | 20.0 | EtOH/80 °C | 5 | 92 | ¹¹¹ |
| 12 | Fe₃O₄@PMO-ICS-ZnO | 10.0 | EtOH/reflux | 3 | 98 | This work |

Table 4. Comparison of the catalytic efficiency of the $\text{Fe}_3\text{O}_4@PMO\text{-ZnO}$ (1) with other heterogeneous or homogeneous catalytic systems for the synthesis of **5a**. Significant values are in bold.

the reaction, $\text{Fe}_3\text{O}_4@PMO\text{-ICS-ZnO}$ catalyst was easily separated from the reaction mixture using an external magnet and the desired product **5** was crystallized by dropwise adding of distilled water to the ethanolic solution. The structure of products **5a–o** was confirmed by melting point as well as FTIR, ¹H NMR and ¹³C NMR spectroscopy.

Conclusions

Novel magnetic $\text{Fe}_3\text{O}_4@PMO\text{-ICS-ZnO}$ nano-ordered catalyst was prepared through a modified environmentally-benign procedure and properly characterized. The catalytic activity of the new thermally stable $\text{Fe}_3\text{O}_4@PMO\text{-ICS-ZnO}$ nanomaterial was demonstrated in the one-pot synthesis of tetrazole derivatives through cascade condensation and concerted 1,3-cycloaddition reactions as a representative of the Click Chemistry concept. Different aromatic aldehydes survived to involve smoothly in the optimized conditions affording the corresponding 5-substituted-1*H*-tetrazole derivatives in high to quantitative yields and good purity. Low catalyst loading, the use of green solvents such as EtOH or water instead of carcinogenic DMF and short reaction time as well as easy separation and recyclability of the catalyst for at least five consecutive runs without significant loss of its activity are notable advantages of this new protocol compared to other recent introduced procedures.

Received: 25 July 2021; Accepted: 19 May 2022

Published online: 24 June 2022

References

- Ugi, I., Domling, A. & Werner, B. Since 1995 the new chemistry of multicomponent reactions and their libraries, including their heterocyclic chemistry. *J. Heterocycl. Chem.* **37**, 647–658 (2000).
- Meghani, N. M., Amin, H. H. & Lee, B.-J. Mechanistic applications of click chemistry for pharmaceutical drug discovery and drug delivery. *Drug Discov. Today* **22**, 1604–1619. <https://doi.org/10.1016/j.drudis.2017.07.007> (2017).

3. Hein, C. D., Liu, X.-M. & Wang, D. Click chemistry, a powerful tool for pharmaceutical sciences. *Pharm. Res.* **25**, 2216–2230 (2008).
4. Tiwari, V. K. *et al.* Cu-catalyzed click reaction in carbohydrate chemistry. *Chem. Rev.* **116**, 3086–3240. <https://doi.org/10.1021/acs.chemrev.5b00408> (2016).
5. Boukis, A. C., Reiter, K., Frölich, M., Hofheinz, D. & Meier, M. A. Multicomponent reactions provide key molecules for secret communication. *Nat. Commun.* **9**, 1–10 (2018).
6. Xiong, Q., Dong, S., Chen, Y., Liu, X. & Feng, X. Asymmetric synthesis of tetrazole and dihydroisoquinoline derivatives by isocyanide-based multicomponent reactions. *Nat. Commun.* **10**, 1–10 (2019).
7. Mardirossian, M. *et al.* D-BMAP18 antimicrobial peptide is active in vitro, resists to pulmonary proteases but loses its activity in a murine model of *Pseudomonas aeruginosa* lung infection. *Front. Chem.* **5**, 40 (2017).
8. Breugst, M. & Reissig, H.-U. The Huisgen reaction: Milestones of the 1,3-dipolar cycloaddition. *Angew. Chem. Int. Ed.* **59**, 12293–12307. <https://doi.org/10.1002/anie.202003115> (2020).
9. Neochoritis, C. G., Zhao, T. & Dömling, A. Tetrazoles via multicomponent reactions. *Chem. Rev.* **119**, 1970–2042. <https://doi.org/10.1021/acs.chemrev.8b00564> (2019).
10. Kang, X.-M., Tang, M.-H., Yang, G.-L. & Zhao, B. Cluster/cage-based coordination polymers with tetrazole derivatives. *Coord. Chem. Rev.* **422**, 213424 (2020).
11. Matthews, D. P., Green, J. E. & Shuker, A. J. Parallel synthesis of alkyl tetrazole derivatives using solid support chemistry. *J. Comb. Chem.* **2**, 19–23 (2000).
12. Bhaskar, V. & Mohite, P. Synthesis, characterization and evaluation of anticancer activity of some tetrazole derivatives. *J. Optoelectron. Biomed. Mater.* **2**, 249–259 (2010).
13. Agalave, S. G., Maujan, S. R. & Pore, V. S. Click chemistry: 1,2,3-Triazoles as pharmacophores. *Chem. Asian J.* **6**, 2696–2718. <https://doi.org/10.1002/asia.201100432> (2011).
14. Hou, J., Liu, X., Shen, J., Zhao, G. & Wang, P. G. The impact of click chemistry in medicinal chemistry. *Expert Opin. Drug Discov.* **7**, 489–501. <https://doi.org/10.1517/17460441.2012.682725> (2012).
15. Heravi, M. M., Zadsirjan, V., Dehghani, M. & Ahmadi, T. Towards click chemistry: Multicomponent reactions via combinations of name reactions. *Tetrahedron* **74**, 3391–3457. <https://doi.org/10.1016/j.tet.2018.04.076> (2018).
16. Pandya, J., Verdia, J. & Joshi, N. An improved novel process for the synthesis of antihypertensive drug, Irbesartan. *Afinidad* **71**, 567 (2014).
17. Koguro, K., Oga, T., Mitsui, S. & Orita, R. Novel synthesis of 5-substituted tetrazoles from nitriles. *Synthesis* **1998**, 910–914 (1998).
18. Konrad, W. *et al.* A combined photochemical and multicomponent reaction approach to precision oligomers. *Chem. A Eur. J.* **24**, 3413–3419 (2018).
19. Kakuchi, R. The dawn of polymer chemistry based on multicomponent reactions. *Polym. J.* **51**, 945–953 (2019).
20. Afshari, R. & Shaabani, A. Materials functionalization with multicomponent reactions: State of the art. *ACS Comb. Sci.* **20**, 499–528 (2018).
21. Ruijter, E., Scheffelaar, R. & Orru, R. V. Multicomponent reaction design in the quest for molecular complexity and diversity. *Angew. Chem. Int. Ed.* **50**, 6234–6246 (2011).
22. Esirden, İ., Erken, E., Kaya, M. & Sen, F. Monodisperse Pt NPs@ rGO as highly efficient and reusable heterogeneous catalysts for the synthesis of 5-substituted 1H-tetrazole derivatives. *Catal. Sci. Technol.* **5**, 4452–4457 (2015).
23. Kritchenkov, A. S. *et al.* Synthesis of novel 1H-tetrazole derivatives of chitosan via metal-catalyzed 1, 3-dipolar cycloaddition. Catalytic and antibacterial properties of [3-(1H-tetrazole-5-yl) ethyl] chitosan and its nanoparticles. *Int. J. Biol. Macromol.* **132**, 340–350 (2019).
24. Varala, R. & Babu, B. H. *Molecular Docking* (IntechOpen, 2018).
25. Ballatore, C., Hurn, D. M. & Smith, A. B. 3rd. Carboxylic acid (bio)isosteres in drug design. *ChemMedChem* **8**, 385–395. <https://doi.org/10.1002/cmdc.201200585> (2013).
26. Zhao, S., Zhang, S., Xu, J. & Hu, L. Synthesis and comparative study of emulsifying and biological properties of triazolated glucolipids. *Tetrahedron* **76**, 131517. <https://doi.org/10.1016/j.tet.2020.131517> (2020).
27. Bakthadoss, M. & Vinayagam, V. Construction of hybrid polycyclic quinolinobenzo [a] phenazine architectures using solid-state melt reaction (SSMR). *Mol. Diver.* **25**, 1–12 (2020).
28. Shelkar, R., Singh, A. & Nagarkar, J. Amberlyst-15 catalyzed synthesis of 5-substituted 1-H-tetrazole via [3+2] cycloaddition of nitriles and sodium azide. *Tetrahedron Lett.* **54**, 106–109. <https://doi.org/10.1016/j.tetlet.2012.10.116> (2013).
29. Duncia, J. V., Pierce, M. E. & Santella, J. B. Three synthetic routes to a sterically hindered tetrazole. A new one-step mild conversion of an amide into a tetrazole. *J. Org. Chem.* **56**, 2395–2400 (1991).
30. Hirata, T. *et al.* Acyliminothiadiazoline derivatives: New, highly potent, and orally active angiotensin II receptor antagonists. *Bioorg. Med. Chem. Lett.* **6**, 1469–1474 (1996).
31. El Anwar, S., Růžicková, Z., Bovol, D., Fojt, L. & Grüner, B. Tetrazole ring substitution at carbon and boron sites of the cobalt Bis(dicarbollide) ion available via dipolar cycloadditions. *Inorg. Chem.* **59**, 17430–17442. <https://doi.org/10.1021/acs.inorgchem.0c02719> (2020).
32. Wei, C.-X., Bian, M. & Gong, G.-H. Tetrazolium compounds: Synthesis and applications in medicine. *Molecules* **20**, 5528–5553 (2015).
33. Abdollahi-Alibeik, M. & Moaddeli, A. Multi-component one-pot reaction of aldehyde, hydroxylamine and sodium azide catalyzed by Cu-MCM-41 nanoparticles: A novel method for the synthesis of 5-substituted 1 H-tetrazole derivatives. *New J. Chem.* **39**, 2116–2122 (2015).
34. Gyoung, Y. S., Shim, J.-G. & Yamamoto, Y. Regiospecific synthesis of 2-allylated-5-substituted tetrazoles via palladium-catalyzed reaction of nitriles, trimethylsilyl azide, and allyl acetates. *Tetrahedron Lett.* **41**, 4193–4196 (2000).
35. Mittal, R. & Awasthi, S. K. Recent advances in the synthesis of 5-substituted 1H-tetrazoles: A complete survey (2013–2018). *Synthesis* **51**, 3765–3783 (2019).
36. Aureggi, V. & Sedelmeier, G. 1,3-Dipolar cycloaddition: Click chemistry for the synthesis of 5-substituted tetrazoles from organoaluminum azides and nitriles. *Angew. Chem. Int. Ed.* **46**, 8440–8444. <https://doi.org/10.1002/anie.200701045> (2007).
37. Li, N.-C. *et al.* Use of angiotensin receptor blockers and risk of dementia in a predominantly male population: Prospective cohort analysis. *BMJ* **340**, b5465 (2010).
38. Bhardwaj, G. How the antihypertensive losartan was discovered. *Expert Opin. Drug Discov.* **1**, 609–618 (2006).
39. De Vogel, S., Hoorn, E. J. & Papademetriou, V. Losartan in cardiovascular disease. *Future Cardiol.* **1**, 433 (2005).
40. Bhatt, U. Five-membered heterocycles with four heteroatoms: Tetrazoles. In *Modern Heterocyclic Chemistry* (ed. Alvarez-Builla, J.) 1401–1430 (Wiley, 2011).
41. Gutmann, B., Roduit, J. P., Roberge, D. & Kappe, C. O. Synthesis of 5-substituted 1H-tetrazoles from nitriles and hydrazoic acid by using a safe and scalable high-temperature microreactor approach. *Angew. Chem. Int. Ed.* **49**, 7101–7105 (2010).
42. Cléménçon, I. F. & Ganem, B. Tandem multicomponent/click reactions: Synthesis of functionalized oxazoles and tetrazoles from acyl cyanides. *Tetrahedron* **63**, 8665–8669 (2007).

43. Nikoorazm, M., Moradi, P. & Noori, N. L-cysteine complex of palladium onto mesoporous channels of MCM-41 as reusable, homoselective and organic–inorganic hybrid nanocatalyst for the synthesis of tetrazoles. *J. Porous Mater.* **27**, 1159–1169. <https://doi.org/10.1007/s10934-020-00894-0> (2020).
44. Moradi, P., Hajjami, M. & Tahmasbi, B. Fabricated copper catalyst on biochar nanoparticles for the synthesis of tetrazoles as antimicrobial agents. *Polyhedron* **175**, 114169. <https://doi.org/10.1016/j.poly.2019.114169> (2020).
45. Jafari, F., Ghorbani-Choghamarani, A. & Hasanzadeh, N. Guanidine complex of copper supported on boehmite nanoparticles as practical, recyclable, chemo and homoselective organic–inorganic hybrid nanocatalyst for organic reactions. *Appl. Organomet. Chem.* **34**, e5901. <https://doi.org/10.1002/aoc.5901> (2020).
46. Himo, F., Demko, Z. P., Noodleman, L. & Sharpless, K. B. Why is tetrazole formation by addition of azide to organic nitriles catalyzed by zinc(II) salts?. *J. Am. Chem. Soc.* **125**, 9983–9987. <https://doi.org/10.1021/ja030204q> (2003).
47. Kantam, M. L., Shiva Kumar, K. B. & Phani Raja, K. An efficient synthesis of 5-substituted 1H-tetrazoles using Zn/Al hydrotalcite catalyst. *J. Mol. Catal. A Chem.* **247**, 186–188. <https://doi.org/10.1016/j.molcata.2005.11.046> (2006).
48. Abrishami, F., Ebrahimikia, M. & Rafee, F. Synthesis of 5-substituted 1H-tetrazoles using a recyclable heterogeneous nanonickel ferrite catalyst. *Appl. Organomet. Chem.* **29**, 730–735. <https://doi.org/10.1002/aoc.3358> (2015).
49. Cantillo, D., Gutmann, B. & Kappe, C. O. Mechanistic insights on azide–nitrile cycloadditions: On the dialkyltin oxide–trimethylsilyl azide route and a new Vilsmeier–Haack-Type Organocatalyst. *J. Am. Chem. Soc.* **133**, 4465–4475. <https://doi.org/10.1021/ja109700b> (2011).
50. Nasrollahzadeh, M., Bayat, Y., Habibi, D. & Moshae, S. FeCl₃–SiO₂ as a reusable heterogeneous catalyst for the synthesis of 5-substituted 1H-tetrazoles via [2+3] cycloaddition of nitriles and sodium azide. *Tetrahedron Lett.* **50**, 4435–4438. <https://doi.org/10.1016/j.tetlet.2009.05.048> (2009).
51. Matloubi Moghaddam, F., Eslami, M. & Ghadirian, N. MCM-41-SO₃H as an efficient reusable nano-ordered heterogeneous catalyst for the synthesis of divers 1- & 5-substituted 1H-tetrazoles. *Sci. Iran.* **26**, 1463–1473. <https://doi.org/10.24200/sci.2018.21088> (2019).
52. Aali, E., Gholizadeh, M. & Noroozi-Shad, N. 1-Disulfo-[2,2-bipyridine]-1,1-dium chloride ionic liquid as an efficient catalyst for the green synthesis of 5-substituted 1H-tetrazoles. *J. Mol. Struct.* **1247**, 131289. <https://doi.org/10.1016/j.molstruc.2021.131289> (2022).
53. Demko, Z. P. & Sharpless, K. B. A Click chemistry approach to tetrazoles by huisgen 1,3-dipolar cycloaddition: Synthesis of 5-sulfonyl tetrazoles from azides and sulfonyl cyanides. *Angew. Chem. Int. Ed.* **41**, 2110–2113. [https://doi.org/10.1002/1521-3773\(20020617\)41:12%3c2110::AID-ANIE2110%3e3.0.CO;2-7](https://doi.org/10.1002/1521-3773(20020617)41:12%3c2110::AID-ANIE2110%3e3.0.CO;2-7) (2002).
54. Demko, Z. P. & Sharpless, K. B. A click chemistry approach to tetrazoles by huisgen 1,3-dipolar cycloaddition: Synthesis of 5-acyltetrazoles from azides and acyl cyanides. *Angew. Chem. Int. Ed.* **41**, 2113–2116. [https://doi.org/10.1002/1521-3773\(20020617\)41:12%3c2113::AID-ANIE2113%3e3.0.CO;2-Q](https://doi.org/10.1002/1521-3773(20020617)41:12%3c2113::AID-ANIE2113%3e3.0.CO;2-Q) (2002).
55. Tisseh, Z. N., Dabiri, M., Nobahar, M., Khavasi, H. R. & Bazgir, A. Catalyst-free, aqueous and highly diastereoselective synthesis of new 5-substituted 1H-tetrazoles via a multi-component domino Knoevenagel condensation/1,3 dipolar cycloaddition reaction. *Tetrahedron* **68**, 1769–1773. <https://doi.org/10.1016/j.tet.2011.12.044> (2012).
56. Demko, Z. P. & Sharpless, K. B. Preparation of 5-substituted 1 H-tetrazoles from nitriles in water. *J. Org. Chem.* **66**, 7945–7950 (2001).
57. Alvim, H. G., da Silva Junior, E. N. & Neto, B. A. What do we know about multicomponent reactions? Mechanisms and trends for the Biginelli, Hantzsch, Mannich, Passerini and Ugi MCRs. *Rsc Adv.* **4**, 54282–54299 (2014).
58. Dekamin, M. G., Azimoshan, M. & Ramezani, L. Chitosan: A highly efficient renewable and recoverable bio-polymer catalyst for the expeditious synthesis of α-amino nitriles and imines under mild conditions. *Green Chem.* **15**, 811–820 (2013).
59. Naeimi, H. & Kiani, F. Ultrasound-promoted one-pot three component synthesis of tetrazoles catalyzed by zinc sulfide nanoparticles as a recyclable heterogeneous catalyst. *Ultrason. Sonochem.* **27**, 408–415 (2015).
60. Xie, L.-G. & Dixon, D. J. Iridium-catalyzed reductive Ugi-type reactions of tertiary amides. *Nat. Commun.* **9**, 1–8 (2018).
61. Khodamorady, M. & Bahrami, K. Fe₃O₄@BNPs-CPTMS-chitosan-Pd(0) as an efficient and stable heterogeneous magnetic nanocatalyst for the chemoselective oxidation of alcohols and homoselective synthesis of 5-substituted 1H-tetrazoles. *ChemistrySelect* **4**, 8183–8194. <https://doi.org/10.1002/slct.201901497> (2019).
62. Hajizadeh, Z., Hassanzadeh-Afruzi, F., Jelodar, D. F., Ahghari, M. R. & Maleki, A. Cu(II) immobilized on Fe₃O₄@HNTs–tetrazole (CFHT) nanocomposite: Synthesis, characterization, investigation of its catalytic role for the 1,3 dipolar cycloaddition reaction, and antibacterial activity. *RSC Adv.* **10**, 26467–26478. <https://doi.org/10.1039/D0RA04772D> (2020).
63. Yuan, X., Wang, Z., Zhang, Q. & Luo, J. An intramolecular relay catalysis strategy for Knoevenagel condensation and 1,3-dipolar cycloaddition domino reactions. *RSC Adv.* **9**, 23614–23621. <https://doi.org/10.1039/C9RA04081A> (2019).
64. Akbarzadeh, P., Koukabi, N. & Kolvari, E. Three-component solvent-free synthesis of 5-substituted-1H-tetrazoles catalyzed by unmodified nanomagnetite with microwave irradiation or conventional heating. *Res. Chem. Intermed.* **45**, 1009–1024. <https://doi.org/10.1007/s11164-018-3657-9> (2019).
65. Safaei-Ghomi, J. & Paymard-Samani, S. Facile and rapid synthesis of 5-substituted 1H-tetrazoles VIA a multicomponent domino reaction using nickel(II) oxide nanoparticles as catalyst. *Chem. Heterocycl. Compd.* **50**, 1567–1574. <https://doi.org/10.1007/s10593-014-1625-x> (2015).
66. Ahmed, N. & Siddiqui, Z. N. Silica molybdic acid catalysed eco-friendly three component synthesis of functionalised tetrazole derivatives under microwave irradiation in water. *RSC Adv.* **5**, 16707–16717. <https://doi.org/10.1039/C5RA01073J> (2015).
67. Tourani, H., Naimi-Jamal, M. R. & Dekamin, M. G. Preparation of 5-substituted-1H-tetrazoles catalyzed by MOFs via two strategies: Direct condensation of aryl nitriles with sodium azide, and tri-component reaction method. *ChemistrySelect* **3**, 8332–8337. <https://doi.org/10.1002/slct.201801392> (2018).
68. Manayil, J. C., Lee, A. F. & Wilson, K. Functionalized periodic mesoporous organosilicas: Tunable hydrophobic solid acids for biomass conversion. *Molecules* **24**, 239 (2019).
69. Ha, C.-S. & Park, S. S. (eds) *Periodic Mesoporous Organosilicas: Preparation, Properties and Applications* 125–187 (Springer, 2019).
70. Van Der Voort, P. *et al.* Periodic mesoporous organosilicas: From simple to complex bridges; a comprehensive overview of functions, morphologies and applications. *Chem. Soc. Rev.* **42**, 3913–3955. <https://doi.org/10.1039/C2CS35222B> (2013).
71. Climent, M. J., Corma, A. & Iborra, S. Heterogeneous catalysts for the one-pot synthesis of chemicals and fine chemicals. *Chem. Rev.* **111**, 1072–1133. <https://doi.org/10.1021/cr1002084> (2011).
72. Li, Z. *et al.* Well-defined materials for heterogeneous catalysis: From nanoparticles to isolated single-atom sites. *Chem. Rev.* **120**, 623–682 (2019).
73. Sharma, V., Orejon, D., Takata, Y., Krishnan, V. & Harish, S. Gladiolus dalenii based bioinspired structured surface via soft lithography and its application in water vapor condensation and fog harvesting. *ACS Sustain. Chem. Eng.* **6**, 6981–6993 (2018).
74. Sheldon, R. A., Arends, I. & Hanefeld, U. *Green Chemistry and Catalysis* (Wiley, 2007).
75. Astruc, D., Lu, F. & Aranzues, J. R. Nanoparticles as recyclable catalysts: The frontier between homogeneous and heterogeneous catalysis. *Angew. Chem. Int. Ed.* **44**, 7852–7872 (2005).
76. Yang, M. M. *et al.* Lack of association of C3 gene with uveitis: Additional insights into the genetic profile of uveitis regarding complement pathway genes. *Sci. Rep.* **7**, 1–8 (2017).

77. Yoshida, M. *et al.* Immobilization of luminescent platinum (II) complexes on periodic mesoporous organosilica and their water reduction photocatalysis. *J. Photochem. Photobiol. A* **358**, 334–344 (2018).
78. Rebbin, V., Schmidt, R. & Fröba, M. Spherical particles of phenylene-bridged periodic mesoporous organosilica for high-performance liquid chromatography. *Angew. Chem. Int. Ed.* **45**, 5210–5214 (2006).
79. Ma, X. *et al.* Hollow periodic mesoporous organosilica nanospheres by a facile emulsion approach. *J. Colloid Interface Sci.* **475**, 66–71 (2016).
80. Cornelius, M., Hoffmann, F. & Fröba, M. Periodic mesoporous organosilicas with a bifunctional conjugated organic unit and crystal-like pore walls. *Chem. Mater.* **17**, 6674–6678 (2005).
81. Wang, W., Grozea, D., Kohli, S., Perovic, D. D. & Ozin, G. A. Water repellent periodic mesoporous organosilicas. *ACS Nano* **5**, 1267–1275 (2011).
82. Zebardasti, A., Dekamin, M. G., Doustkhah, E. & Assadi, M. H. N. Carbamate-isocyanurate-bridged periodic mesoporous organosilica for van der Waals CO₂ capture. *Inorg. Chem.* **59**, 11223–11227. <https://doi.org/10.1021/acs.inorgchem.0c01449> (2020).
83. Karimi, B. & Esfahani, F. K. Unexpected golden Ullmann reaction catalyzed by Au nanoparticles supported on periodic mesoporous organosilica (PMO). *Chem. Commun.* **47**, 10452–10454 (2011).
84. Borah, P., Ma, X., Nguyen, K. T. & Zhao, Y. A vanadyl complex grafted to periodic mesoporous organosilica: A green catalyst for selective hydroxylation of benzene to phenol. *Angew. Chem.* **124**, 7876–7881 (2012).
85. Yaghoobi, A., Dekamin, M. G., Arefi, E. & Karimi, B. Propylsulfonic acid-anchored isocyanurate-based periodic mesoporous organosilica (PMO-ICS-Pr-SO₃H): A new and highly efficient recoverable nanoporous catalyst for the one-pot synthesis of bis(indolyl)methane derivatives. *J. Colloid Interface Sci.* **505**, 956–963. <https://doi.org/10.1016/j.jcis.2017.06.055> (2017).
86. Dekamin, M. G., Arefi, E. & Yaghoobi, A. Isocyanurate-based periodic mesoporous organosilica (PMO-ICS): A highly efficient and recoverable nanocatalyst for the one-pot synthesis of substituted imidazoles and benzimidazoles. *RSC Adv.* **6**, 86982–86988. <https://doi.org/10.1039/C6RA14550G> (2016).
87. Akbari, A., Dekamin, M. G., Yaghoobi, A. & Naimi-Jamal, M. R. Novel magnetic propylsulfonic acid-anchored isocyanurate-based periodic mesoporous organosilica (Iron oxide@PMO-ICS-PrSO₃H) as a highly efficient and reusable nanoreactor for the sustainable synthesis of imidazopyrimidine derivatives. *Sci. Rep.* **10**, 10646. <https://doi.org/10.1038/s41598-020-67592-4> (2020).
88. Zebardasti, A., Dekamin, M. G. & Doustkhah, E. The isocyanurate-carbamate-bridged hybrid mesoporous organosilica: An exceptional anchor for Pd nanoparticles and a unique catalyst for nitroaromatics reduction. *Catalysts* **11**, 621 (2021).
89. Valiey, E. & Dekamin, M. G. Pyromellitic diamide–diacid bridged mesoporous organosilica nanospheres with controllable morphologies: A novel PMO for the facile and expeditious synthesis of imidazole derivatives. *Nanoscale Adv.* **4**, 294–308. <https://doi.org/10.1039/D1NA00738F> (2022).
90. Valiey, E. & Dekamin, M. G. Supported copper on a diamide–diacid-bridged PMO: An efficient hybrid catalyst for the cascade oxidation of benzyl alcohols/Knoevenagel condensation. *RSC Adv.* **12**, 437–450. <https://doi.org/10.1039/D1RA06509B> (2022).
91. Yoo, C. G., Pu, Y. & Ragauskas, A. J. Ionic liquids: Promising green solvents for lignocellulosic biomass utilization. *Curr. Opin. Green Sustain. Chem.* **5**, 5–11 (2017).
92. Alzeer, M. I. & MacKenzie, K. J. Synthesis and catalytic properties of new sustainable aluminosilicate heterogeneous catalysts derived from fly ash. *ACS Sustain. Chem. Eng.* **6**, 5273–5282 (2018).
93. Liu, L. & Corma, A. Metal catalysts for heterogeneous catalysis: From single atoms to nanoclusters and nanoparticles. *Chem. Rev.* **118**, 4981–5079 (2018).
94. Cuenya, B. R. & Behafarid, F. Nanocatalysis: Size- and shape-dependent chemisorption and catalytic reactivity. *Surf. Sci. Rep.* **70**, 135–187 (2015).
95. Hatton, B., Landskron, K., Whitnall, W., Perovic, D. & Ozin, G. A. Past, present, and future of periodic mesoporous organosilicas the PMOs. *Acc. Chem. Res.* **38**, 305–312 (2005).
96. Chanson, R. *et al.* Damage-free plasma etching of porous organo-silicate low-k using micro-capillary condensation above – 50 °C. *Sci. Rep.* **8**, 1–12 (2018).
97. Park, S. S., Moorthy, M. S. & Ha, C.-S. Periodic mesoporous organosilicas for advanced applications. *NPG Asia Mater.* **6**, e96 (2014).
98. Shokrian, M., Sadrzadeh, M. & Mohammadi, T. C₃H₈ separation from CH₄ and H₂ using a synthesized PDMS membrane: Experimental and neural network modeling. *J. Membr. Sci.* **346**, 59–70 (2010).
99. Valimaña-Traverso, J. *et al.* Periodic mesoporous organosilica materials as sorbents for solid-phase extraction of drugs prior to simultaneous enantiomeric separation by capillary electrophoresis. *J. Chromatogr. A* **1566**, 135–145 (2018).
100. Wu, L. *et al.* Sulfonated periodic-mesoporous-organosilicas column for selective separation of C₂H₂/CH₄ mixtures. *J. Solid State Chem.* **264**, 113–118 (2018).
101. Teng, Z. *et al.* A facile multi-interface transformation approach to monodisperse multiple-shelled periodic mesoporous organosilica hollow spheres. *J. Am. Chem. Soc.* **137**, 7935–7944 (2015).
102. Ha, C.-S. & Park, S. S. *Periodic Mesoporous Organosilicas* 87–100 (Springer, 2019).
103. Elhamifar, D. & Ardehshirfar, H. Phenyl and ionic liquid based bifunctional periodic mesoporous organosilica supported copper: An efficient nanocatalyst for clean production of polyhydroquinolines. *J. Colloid Interface Sci.* **505**, 1177–1184 (2017).
104. Yang, Q., Liu, J., Zhang, L. & Li, C. Functionalized periodic mesoporous organosilicas for catalysis. *J. Mater. Chem.* **19**, 1945–1955 (2009).
105. Huang, J., Zhang, F. & Li, H. Organometal-bridged PMOs as efficiency and reusable bifunctional catalysts in one-pot cascade reactions. *Appl. Catal. A* **431**, 95–103 (2012).
106. Hoffmann, F., Cornelius, M., Morell, J. & Fröba, M. Periodic mesoporous organosilicas (PMOs): Past, present, and future. *J. Nanosci. Nanotechnol.* **6**, 265–288 (2006).
107. Olivieri, F., Castaldo, R., Cocca, M., Gentile, G. & Lavorgna, M. Mesoporous silica nanoparticles as carriers of active agents for smart anticorrosive organic coatings: A critical review. *Nanoscale* **13**, 9091–9111. <https://doi.org/10.1039/D1NR01899J> (2021).
108. Hasanzadeh Banakar, S., Dekamin, M. G. & Yaghoobi, A. Selective and highly efficient synthesis of xanthenedione or tetraketone derivatives catalyzed by ZnO nanorod-decorated graphene oxide. *N. J. Chem.* **42**, 14246–14262. <https://doi.org/10.1039/C8NJ01053F> (2018).
109. Davoodi, F., Dekamin, M. G. & Alirezvani, Z. A practical and highly efficient synthesis of densely functionalized nicotinonitrile derivatives catalyzed by zinc oxide-decorated superparamagnetic silica attached to graphene oxide nanocomposite. *Appl. Organomet. Chem.* **33**, e4735. <https://doi.org/10.1002/aoc.4735> (2019).
110. Behloul, C., Benlahrech, M., Foubelo, F., Nájera, C. & Yus, M. Indium-, magnesium-, and zinc-mediated debenzoylation of protected 1H-tetrazoles: A comparative study. *Synthesis* **50**, 3430–3435 (2018).
111. Yuan, X., Wang, Z., Zhang, Q. & Luo, J. An intramolecular relay catalysis strategy for Knoevenagel condensation and 1, 3-dipolar cycloaddition domino reactions. *RSC Adv.* **9**, 23614–23621 (2019).
112. Tisseh, Z. N., Dabiri, M., Nobahar, M., Khavasi, H. R. & Bazgir, A. Catalyst-free, aqueous and highly diastereoselective synthesis of new 5-substituted 1H-tetrazoles via a multi-component domino Knoevenagel condensation/1, 3 dipolar cycloaddition reaction. *Tetrahedron* **68**, 1769–1773 (2012).
113. Bakherad, M., Doosti, R., Keivanloo, A., Gholizadeh, M. & Jadidi, K. Rapid, green, and catalyst-free one-pot three-component syntheses of 5-substituted 1H-tetrazoles in magnetized water. *J. Iran. Chem. Soc.* **14**, 2591–2597 (2017).

114. Parmar, B. D. *et al.* A base-catalyzed, domino aldol/hetero-Diels–Alder synthesis of tricyclic pyrano [3, 4-c] chromenes in glycerol. *J. Org. Chem.* **81**, 4955–4964 (2016).
115. Safaei-Ghomi, J., Paymard-Samani, S., Zahedi, S. & Shahbazi-Alavi, H. Sonochemical synthesis of 5-substituted 1H-tetrazoles catalyzed by ZrP₂O₇ nanoparticles and regioselective conversion into new 2, 5-disubstituted tetrazoles. *Z. für Nat. B* **70**, 819–828 (2015).
116. Bonnamour, J. & Bolm, C. Iron salts in the catalyzed synthesis of 5-substituted 1H-tetrazoles. *Chem. A Eur. J.* **15**, 4543–4545 (2009).
117. Chattopadhyay, B., Vera, C. I. R., Chuprakov, S. & Gevorgyan, V. Fused tetrazoles as azide surrogates in click reaction: Efficient synthesis of N-heterocycle-substituted 1, 2, 3-triazoles. *Org. Lett.* **12**, 2166–2169 (2010).
118. Chermahini, A. N. *et al.* Clay-catalyzed synthesis of 5-substituent 1-H-tetrazoles. *J. Heterocycl. Chem.* **47**, 913–922 (2010).
119. Heravi, M. M., Fazeli, A., Oskooie, H. A., Beheshtiha, Y. S. & Valizadeh, H. Click synthesis of 5-substituted 1H-tetrazoles from aldehydes, hydroxylamine, and [bmim] N₃ via one-pot, three-component reaction. *Synlett* **23**, 2927–2930 (2012).
120. Khaghaninejad, S., Heravi, M. M., Hosseinejad, T., Oskooie, H. A. & Bakavoli, M. Regio-selective synthesis of 5-substituted 1H-tetrazoles using ionic liquid [BMIM] N₃ in solvent-free conditions: A click reaction. *Res. Chem. Intermed.* **42**, 1593–1610 (2016).
121. Fazeli, A. *et al.* Heteropolyacid catalyzed click synthesis of 5-substituted 1H-tetrazoles from [bmim] N₃ and nitriles under solvent-free conditions. *Monatshefte für Chem.-Chem. Month.* **144**, 1407–1410 (2013).
122. Olkhovik, O. & Jaroniec, M. Periodic mesoporous organosilica with large heterocyclic bridging groups. *J. Am. Chem. Soc.* **127**, 60–61. <https://doi.org/10.1021/ja043941a> (2005).

Acknowledgements

The authors thank The Research Council of Iran University of Science and Technology (IUST), Tehran, Iran (Grant No 160/20969) for their support. We would also like to acknowledge the support of Iran Nanotechnology Initiative Council (INIC), Iran.

Author contributions

S.S. worked on the topic as her MSc. thesis and prepared the initial draft of the manuscript. M.G.D. is the supervisor of both S.S. and A.A. as his MSc. students. Also, he edited and revised the manuscript completely. A.A. worked closely with S.S. for doing experimental section and interpreting of the characterization data. M.R.N.-J. is the advisor of S.S. and the supervisor of A.A. He also helped to interpret data and edited the manuscript partially.

Competing interests

The authors declare no competing interests.

Additional information

Supplementary Information The online version contains supplementary material available at <https://doi.org/10.1038/s41598-022-13011-9>.

Correspondence and requests for materials should be addressed to M.G.D.

Reprints and permissions information is available at www.nature.com/reprints.

Publisher's note Springer Nature remains neutral with regard to jurisdictional claims in published maps and institutional affiliations.



Open Access This article is licensed under a Creative Commons Attribution 4.0 International License, which permits use, sharing, adaptation, distribution and reproduction in any medium or format, as long as you give appropriate credit to the original author(s) and the source, provide a link to the Creative Commons licence, and indicate if changes were made. The images or other third party material in this article are included in the article's Creative Commons licence, unless indicated otherwise in a credit line to the material. If material is not included in the article's Creative Commons licence and your intended use is not permitted by statutory regulation or exceeds the permitted use, you will need to obtain permission directly from the copyright holder. To view a copy of this licence, visit <http://creativecommons.org/licenses/by/4.0/>.

© The Author(s) 2022